Journal of Power Sources 196 (2011) 5779–5783

Contents lists available at ScienceDirect

Journal of Power Sources

journal homepage: www.elsevier.com/locate/jpowsour

Short communication

Optimization of MnO_2/vertically aligned carbon nanotube composite for supercapacitor application

Roger Amade*, Eric Jover, Burak Caglar, Toygan Mutlu, Enric Bertran

Department of Applied Physics and Optics, FEMAN Group, IN2UB, Universitat de Barcelona, c/Martí i Franquès 1, 08028 Barcelona, Spain

ARTICLE INFO

Article history:
Received 15 October 2010
Received in revised form
24 December 2010
Accepted 13 February 2011
Available online 21 February 2011

Keywords:
Carbon nanotube
Plasma enhanced chemical vapour deposition
Supercapacitor
Electrochemical properties
Manganese oxide

ABSTRACT

The optimization strategy for producing manganese oxide supercapacitors based on vertically aligned carbon nanotubes (VACNTs) deposited on large area electrodes is presented. A single sequential process of sputtering, annealing and plasma enhanced chemical vapour deposition (PECVD) is applied to produce dense and uniform VACNTs electrodes. As dielectric layer of the supercapacitor, manganese oxide is electrodeposited lining the surface of the VACNTs electrodes. The control of the growing parameters such as catalyst thickness layer, temperature and deposition time for tuning the density, length and diameter of the VACNTs and their structure are found to be key points for the optimization of the MnO_2 electrodeposition process in view to improve the efficiency of the supercapacitor devices.

The electrochemical properties of the obtained electrodes are characterized using cyclic voltammetry and galvanostatic charge–discharge techniques. A specific capacitance of 642 Fg^{-1} is obtained for MnO_2/VACNTs nanocomposite electrode at a scan rate of 10 mV s^{-1}.

1. Introduction

Supercapacitors as energy storage devices fill the gap between conventional batteries and capacitors, i.e. they have high specific energy and power density [1]. The separation of electrical charge in a supercapacitor can be associated with the build up of an electrical double layer at the interface between electrode and electrolyte and/or with the transfer of electrons between the electrolyte and the surface of the electrode. The latter mechanism (pseudocapacitance) is a faradaic process related with a change in the oxidation state of the electrode [1].

Advances in nanotechnology and particularly in the fabrication of carbon nanotubes (CNTs) have helped the development of more efficient supercapacitors [2,3]. Due to their large surface area (1 to >2000 $m^2 g^{-1}$), electrical, thermal and mechanical properties, CNTs have a potential application in hydrogen storage devices [4], lithium batteries, fuel cells and energy storage devices [5]. Several methods such as chemical vapour deposition (CVD), laser ablation, or arc discharge have been studied for their synthesis [6]. However, we highlight the particular characteristics of CNTs grown by plasma enhanced chemical vapour deposition (PECVD) [7,8]. In this regard, dense, well ordered and vertically aligned carbon nanotubes (VACNTs), inserted to the substrate electrode, with an internal structure "bamboo", which leads to high electron transfer in electrochemical processes, are key points for improving the functional characteristics of supercapacitors.

The addition of a metal oxide on the carbonaceous substrate increases the electrochemical performance of the electrode material. Highest specific capacitance values have been reported for RuO_2/CNTs nanocomposite [9], but its high cost and environmental harmfulness limits its application. Thus, other oxides are being extensively studied as possible dielectric materials in supercapacitor devices such as V_2O_5 [10], MnO_2 [11–13] and NiO [14]. Among them, manganese dioxide exhibits promising electrochemical properties, has a lower cost and is considered environmentally friendlier than other metal transition oxides. The combination of CNTs and MnO_2 has already been reported for its use as supercapacitors [11,12,15–25]. However, almost all these reports deal with misaligned and disordered CNTs and do not optimize their morphology. At the best of our knowledge only very few authors have reported the use of vertically aligned CNTs in combination with MnO_2 [17,26–28]. VACNTs-based electrodes present several advantages with respect to non-aligned ones; low contact resistance, large specific surface area, fast electron transfer kinetics, low capacitive currents and they can be confined to a desired area by photolithography among others.

The goal of the present work is to optimize the parameters of PECVD and electrodeposition processes in order to obtain dense, long and vertically aligned carbon nanotubes with a high specific surface area and a suitable superstructure forming a thin layer of

* Corresponding author. Tel.: +34 93 403 7089; fax: +34 93 403 9219.
E-mail address: r.amade@ub.edu (R. Amade).

0378-7753/$ – see front matter © 2011 Elsevier B.V. All rights reserved.
doi:10.1016/j.jpowsour.2011.02.029

manganese oxide lining the surface of the CNTs. These key features enhance the functionality of MnO_2/VACNTs supercapacitors, as shown in this report.

2. Experimental

2.1. Growth of vertically aligned carbon nanotubes

The production of VACNTs was carried out in a multiple reactor chamber having two magnetron sputtering heads, with 3″ targets, one port for annealing treatment and one cathode for PECVD. The system was designed for growing dense and homogeneous CNTs on Fe catalyst nanoparticles deposited on 2″ c-Si wafers in a single vacuum run. This has the advantage of avoiding surface oxidation of the catalyst. During the first step a thin layer (a few nanometers thick) of Fe catalyst is sputtered on a p-type boron doped silicon wafer (0.01–0.02 Ω cm range). Afterwards, the sample is annealed under hydrogen to obtain Fe nanoislands. Then the precursor gas (NH_3, 0.8 mbar, 100 sccm) and the carbon precursor (C_2H_2, 1 mbar, 50 sccm) are allowed to enter the reactor chamber and the PECVD reaction takes place with the formation of CNTs. During annealing time and PECVD the sample was heated a PID Xantrex heater (XDC 60-100) controlled by a pyrometer. Three vacuum pumps were used; rotatory pump (EV25 QS AL, Leybold Vacuum GmbH, Germany), root pump (WU 251, Leybold Heraeus RUVAC, Germany) and turbomolecular pump (Turbovac 361 C, Leybold Vacuum GmbH, Germany). The pressure was kept constant during each process by a MKS 651 Controller and a variable conductance valve.

2.2. Electrochemical deposition of MnO_2

The electrochemical deposition was carried out using two different methods; potentiostatic and galvanostatic.

The potentiostatic deposition was performed in a three electrode cell system, using an Ag/AgCl reference electrode (3 M KCl), a Pt-ring counter electrode and the CNTs as working electrode. A 0.2 M $MnSO_4{\cdot}H_2O$ solution was used for the anodic deposition of MnO_2. The optimum conditions obtained in this work were: 0.6 V applied potential and 3 min of deposition time.

The galvanostatic method was carried out in order to better control the deposition of the manganese oxide layer. In this case, a two electrode cell was used [17]. The CNTs electrode was used as the anode and a graphite electrode as the cathode. About 0.5 cm^3 of a 0.2 M $MnSO_4{\cdot}H_2O$ solution was introduced drop wise through a hole in the cathode during the deposition, as explained by Fan and co-workers [17]. The optimum conditions were found to be a constant current of 1 mA cm^{-2} and 2 min of deposition time.

A quantitative analysis of the amount of manganese dioxide galvanostatically deposited on the nanotubes was performed by oxidizing the sample to MnO^{4-} and measuring its absorbency at 525 nm [18]. The concentration of permanganate ions was obtained from UV–vis spectrophotometry and the loading mass of MnO_2 was calculated from this value, which equalled 16 μg and corresponds to about 20 nm of thickness.

2.3. Electrochemical characterization of CNTs/MnO_2 nanocomposite electrode

The electrochemical properties of the obtained electrodes were characterized in a typical three electrode cell using Ag/AgCl (3 M KCl) as a reference electrode, a Pt-ring as a counter electrode and CNTs/MnO_2 nanocomposite as the working electrode with a geometrical area of 1 cm^2. Cyclic voltammetry (CV) and galvanostatic charge–discharge measurements were carried out in a 0.2 M Na_2SO_4 solution. All electrochemical measurements were performed using a potentiostat/galvanostat (AutoLab, PGSTAT30, USA).

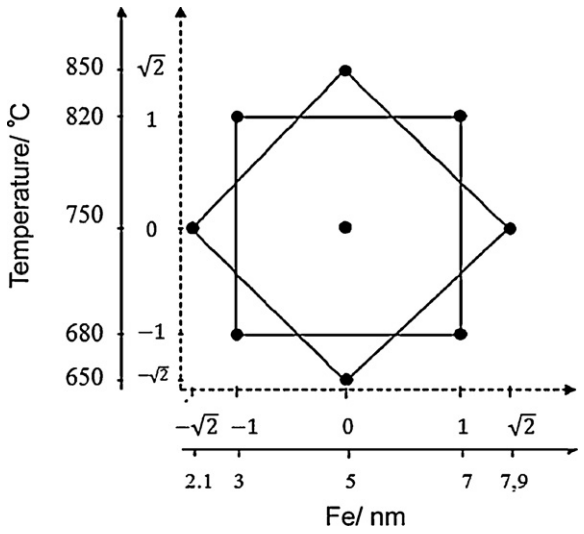

Fig. 1. Box–Wilson experimental design samples distribution for two main parameters (reaction temperature and Fe catalyst thickness).

Table 1
Smmary of the optimum found operational parameters.

Parameter	Value
Catalyst layer thickness	3 nm
Annealing time	870 s
PECVD process temperature	680 °C
PECVD process plasma power	RF 50 W
PECVD process time	900 s

3. Results and discussion

3.1. Optimization of the growth parameters

The optimization of the PECVD process parameters was based on a Box–Wilson experimental design (see Fig. 1). This experimental design enables to simultaneously optimize two parameters taking into account their interactions. Based on previous works, PECVD process temperature and catalyst layer thickness were selected for their optimization. As dependent variables CNTs alignment, density, length and diameter were considered. Central point was replicated 5 times in order to evaluate the intrinsic standard deviation of the process.

Based on these experiments, which were carried out in a random order, a second degree polynomial equation was adjusted for the tested dependent variables (Eq. (1)).

$$A = a_0 + a_1 t + a_2 T + a_3 tT + a_4 t^2 + a_5 T^2 \quad (1)$$

where A is a dependent magnitude, α_n are constant coefficients, t is the Fe layer thickness and T the PECVD process temperature. The α_n coefficients were adjusted using SPSS 16.0 (Chicago (IL), USA) multiple linear regression tool.

As an example, for the CNTs density dependent magnitude (arbitrary units), the polynomial model was found to be statistically significant ($p < 0.05$) explaining 85% of the samples variation with $\alpha_0 = -2.8$, $\alpha_1 = -8.5$, $\alpha_2 = 0.11$, $\alpha_3 = 0.01$, $\alpha_4 = 0.06$, $\alpha_5 = -0.0001$.

Afterwards, other PECVD parameters were optimized individually such as annealing time and PECVD process time. A summary of the selected parameter values is given in Table 1. Typically, vertically aligned nanotubes with about 30 nm in diameter, 10 μm in length and a CNTs density around 10^{10} cm^{-2} were obtained.

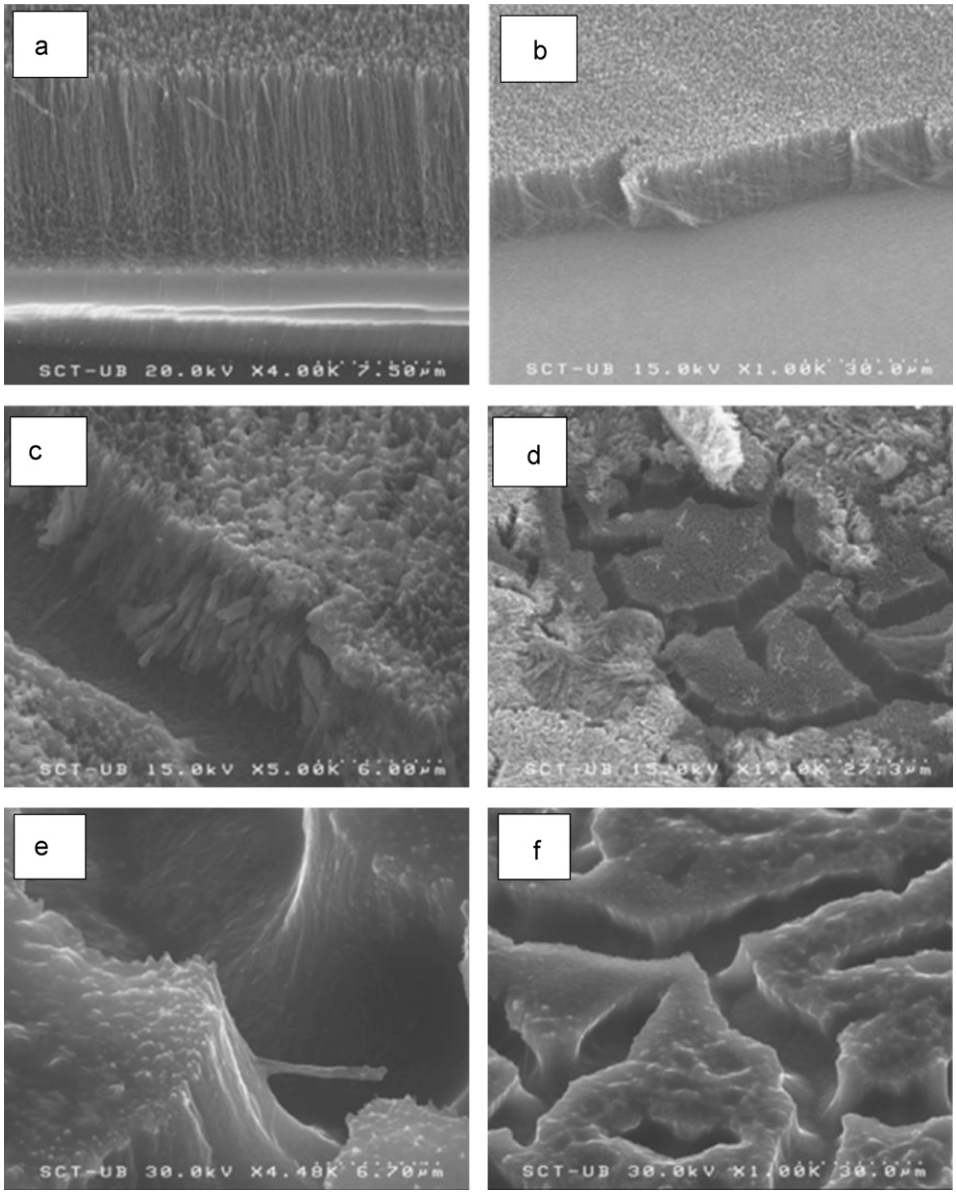

Fig. 2. SEM images of a forest of long, dense and vertically aligned CNTs obtained under optimum PECVD conditions (a) and (b). SEM images of potentiostatic-deposited MnO_2 on CNTs (c) and (d). SEM images of galvanostatic-deposited MnO_2 on CNTs (e) and (f).

3.2. Morphological characterization

The morphology and structure of the obtained CNTs were systematically analyzed by means of scanning electron microscopy (SEM) (HITACHI S 2300, Japan) and transmission electron microscopy (TEM) (Philips CM-30, The Netherlands) during the optimization process. The quality of the carbon nanotubes was studied by means of Raman spectroscopy (HORIBA Jobin Yvon T 64000, Japan).

Fig. 2a and b show SEM images of long and dense VACNTs obtained using optimum PECVD process conditions. After potentiostatic deposition of MnO_2 the carbon nanotubes are covered with a thick and non-homogeneous layer of manganese dioxide as seen in Fig. 2c and d. A thinner and more homogeneous layer of MnO_2 lining the surface of the CNTs is obtained by galvanostatic deposition of the oxide (see Fig. 2e and f).

TEM images of the nanotubes (Fig. 3) reveal multi-wall CNTs (MWNT) with a bamboo-like structure. This is particularly interesting in the fabrication of electrodes since the elevated active surface area allows a higher electron exchange between the solution and the graphitic planes of the nanotubes. In fact, it has been proven [29,30] that the carbon atoms at the tips of the graphitic planes in bamboo-like structured CNTs, are more reactive.

Raman spectroscopy measurements of the obtained carbon nanotubes show typical D (1332 cm^{-1}) and G (1580 cm^{-1}) bands [31] (Fig. 4). The Raman spectra also confirms the presence of MWNT since for single wall carbon nanotubes (SWNT) a multi-peak feature of the *G* band is expected, which does not appear [32,33]. The *G* band corresponds to the symmetric E_{2g} vibrational mode in graphite-like materials [34], while the *D* band is related with structural disorder of the nanotubes [31]. The intensity ratio between the *D* and the *G* band is 0.84 which points to a considerable disorder of CNT walls associated to the bamboo structure. This could be a consequence of the opening of crystal planes of graphene, which would favour a higher electronic transfer of the walls of the CNTs [8].

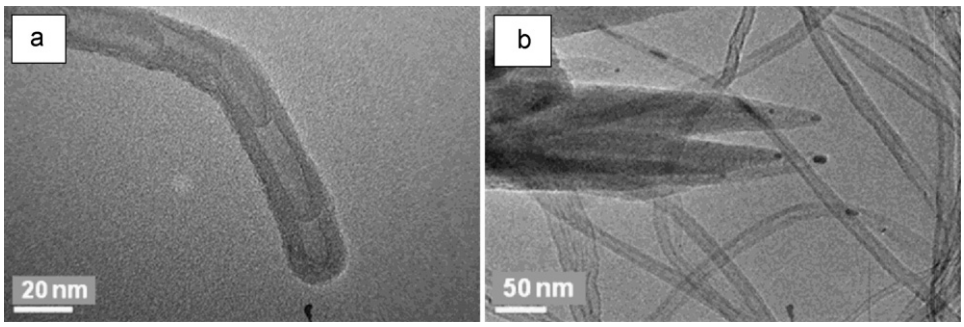

Fig. 3. (a) TEM image of MWCNTs obtained under optimum PECVD conditions showing bamboo-like structure. (b) TEM image showing the Fe catalyst particle on the tips of the nanotubes.

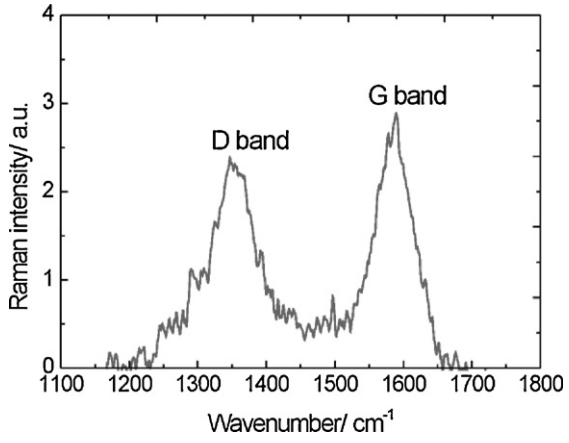

Fig. 4. Raman spectra of obtained vertically aligned carbon nanotubes showing the *D* and *G* bands at approximately 1332 cm^{-1} and 1580 cm^{-1}, respectively.

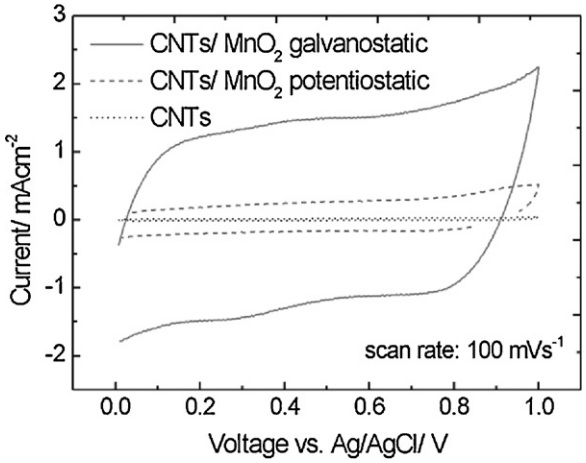

Fig. 5. Comparison between the cyclic voltammograms of bare CNTs, CNTs/MnO_2-p and CNTs/MnO_2-g at 100 mV s^{-1} scan rate in 0.2 M Na_2SO_4 solution.

3.3. Electrochemical characterization of the CNTs/MnO_2 electrodes

The average specific capacitance of the electrodes was calculated from the cyclic voltammograms of the samples according to Eq. (2):

$$C_s = \frac{q_a + |q_c|}{2m\Delta V} \quad (2)$$

where C_s is the specific capacitance in Fg^{-1}, ΔV is the voltage window in V and m is the mass of the electrodeposited MnO_2 layer in g. q_a and q_c are the anodic and cathodic charge, respectively, in C.

Fig. 5 shows a comparison between the cyclic voltammograms of potentiostatic – deposited MnO_2 on CNTs (CNTs/MnO_2-p), galvanostatic – deposited MnO_2 on CNTs (CNTs/MnO_2-g) and bare CNTs at a scan rate of 100 mV s^{-1}. As expected, the galvanostatic method presents better results than the potentiostatic method, while bare CNTs have the lowest capacitance. The specific capacitance of the CNTs/MnO_2-g electrode obtained at 10 mV s^{-1} scan rate is 642 Fg^{-1}, which is much higher than other values reported in the literature for activated carbon/MnO_2 electrodes [35,36]. Therefore, it is proven that CNTs are a suitable template to deposit manganese oxide, mainly due to their high surface area and conductivity. On the other hand, 642 Fg^{-1} at 10 mV s^{-1} corresponds to about 60% of the theoretical capacitance of MnO_2, which is 1100 Fg^{-1} [25]. In order to increase the specific capacitance of the supercapacitor a thinner layer of MnO_2 should be deposited covering a nanostructured electrode with a large specific surface area like, e.g., VACNTs.

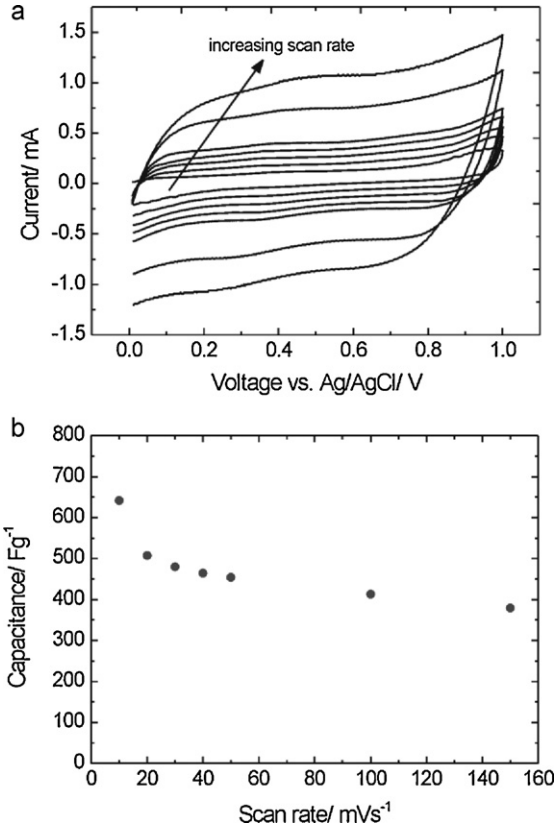

Fig. 6. (a) Cyclic voltammograms of a CNTs/MnO_2-g electrode at several scan rates (from 5 mV s^{-1} to 150 mV s^{-1}) in 0.2 M Na_2SO_4 solution. (b) Specific capacitance versus scan rate of the CNTs/MnO_2-g electrode.

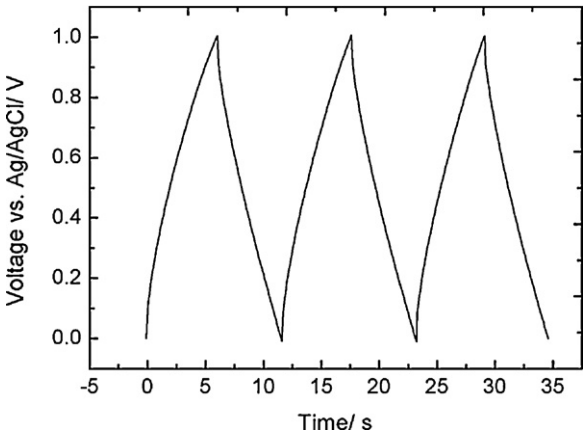

Fig. 7. Constant current charge/discharge curves of a CNTs/MnO_2-g sample in 0.2 M Na_2SO_4 solution obtained at a current density of 1 mA cm^{-2}.

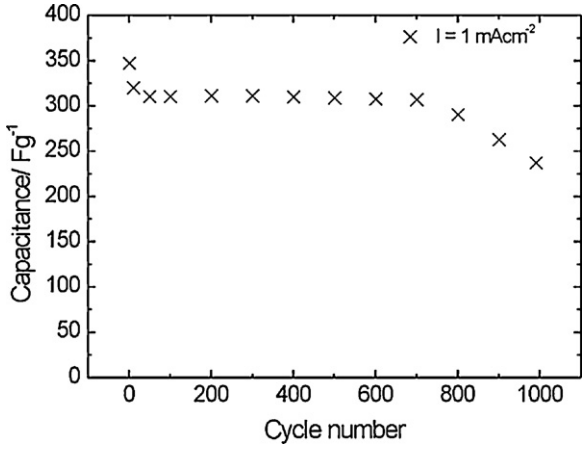

Fig. 8. Cycle stability of a CNTs/MnO_2-g nanocomposite electrode in 0.2 M Na_2SO_4 solution obtained from discharge curves at a current density of 1 mA cm^{-2}.

Furthermore the CNTs/MnO_2-g electrode show rectangular-shaped cyclic voltammograms without clear redox peaks at different scan rates (from 10 mV s^{-1} to 150 mV s^{-1}), which is important for supercapacitive applications (see Fig. 6).

The cycling stability of the CNTs/MnO_2-g nanocomposite electrodes was studied by applying galvanostatic charge/discharge cycles at a current density of 1 mA cm^{-2} in a 0.2 M Na_2SO_4 solution as shown in Fig. 7. The specific capacitance of the electrodes was calculated from the slope of the discharge curves applying the following equation:

$$C_s = \frac{I}{(\Delta V/\Delta t)m} \quad (3)$$

where C_s and m have the same meaning and units as in Eq.2. ΔV is the voltage difference during the discharge in V, I is the current applied in A and Δt is the discharge time in s.

The electrodes show good stability during the first 800 cycles at a current density of 1 mA cm^{-2}, as observed in Fig. 8. Afterwards, the specific capacitance starts to decrease which indicates the presence of irreversible reactions at the surface of the electrode.

4. Conclusion

Using a Box–Wilson experimental design, dense, long and VACNTs deposits have been obtained under optimum conditions. It has been shown that galvanostatic deposition of manganese oxide using VACNTs as anode electrode provides better capacitive performance than potentiostatically deposited manganese oxide on VACNTs. A specific capacitance of 642 Fg^{-1} was obtained for CNTs/MnO_2-g nanocomposite electrode in 0.2 M Na_2SO_4 aqueous solution at a scan rate of 10 mV s^{-1}. The specific capacitance of the electrode has good stability during the first 800 cycles at a current density of 1 mA cm^{-2}.

Acknowledgements

This study was supported by projects 2009SGR00185 of AGAUR of Generalitat de Catalunya and CTQ2009-14674-C02-01 of MICINN of Spain. The authors thank to Serveis Científico-tècnics of the Universitat de Barcelona (SCT-UB) for measurement facilities, Dr. Carles Corbella, Dr. Oriol Arteaga and Noemí Aguiló for their help throughout the work.

References

[1] P. Simon, Y. Gogotsi, Nat. Mater. 7 (2008) 845–854.
[2] J.H. Chen, W.Z. Li, D.Z. Wang, S.X. Yang, J.G. Wen, Z.F. Ren, Carbon 40 (2002) 1193–1197.
[3] B.-J. Yoon, S.-H. Jeong, K.-H. Lee, H.S. Kim, C.G. Park, J.H. Han, Chem. Phys. Lett. 388 (2004) 170–174.
[4] A.C. Dillon, K.M. Jones, T.A. Bekkedahl, C.H. Klang, D.S. Bethune, M.J. Heben, Nature 386 (1997) 377–379.
[5] A.S. Aricò, P. Bruce, B. Scrosati, J.-M. Tarascon, W. Schalkwijk, Nat. Mater. 4 (2005) 366–377.
[6] M. Paradise, T. Goswami, Mater. Des. 28 (2007) 1477–1489.
[7] J. García-Céspedes, M. Rubio-Roy, M.C. Polo, E. Pascual, J.L. Andujar, E. Bertran, Diam. Relat. Mater. 16 (2007) 1131–1135.
[8] F. Javier del Campo, J. García-Céspedes, F. Xavier Muñoz, E. Bertran, Electrochem. Commun. 10 (2008) 1242–1245.
[9] I.-H. Kim, J.-H. Kim, Y.-H. Lee, K.-B. Kim, J. Electrochem. Soc. 152 (2005) A2170–A2178.
[10] I.-H. Kim, J.-H. Kim, B.-W. Cho, Y.-H. Lee, K.-B. Kim, J. Electrochem. Soc. 153 (2006) A989–A996.
[11] Z. Fan, J. Chen, M. Wang, K. Cui, H. Zhou, Y. Kuang, Diam. Relat. Mater. 15 (2006) 1478–1483.
[12] S.-B. Ma, K.-W. Nam, W.-S. Yoon, X.-Q. Yang, K.-Y. Ahn, K.-H. Oh, K.-B. Kim, J. Power Sources 178 (2008) 483–489.
[13] C.Y. Lee, H.M. Tsai, H.J. Chuang, S.Y. Li, P. Lin, T.Y. Tseng, J. Electrochem. Soc. 152 (2005) A716–A720.
[14] J.Y. Lee, K. Liang, K.H. An, Y.H. Lee, Synth. Mater. 150 (2005) 153–157.
[15] C.-Y. Chen, T.-C. Chien, Y.-C. Chan, C.-K. Lin, S.-C. Wang, Diam. Relat. Mater. 18 (2009) 482–485.
[16] S.-L. Chou, J.-Z. Wang, S.-Y. Chew, H.-K. Liu, S.-X. Dou, Electrochem. Commun. 10 (2008) 1724–1727.
[17] Z. Fan, J. Chen, B. Zhang, B. Liu, X. Zhong, Y. Kuang, Diam. Relat. Mater. 17 (2008) 1943–1948.
[18] Z. Fan, J. Chen, B. Zhang, F. Sun, B. Liu, Y. Kuang, Mater. Res. Bull. 43 (2008) 2085–2091.
[19] J.M. Ko, K.M. Kim, Mater. Chem. Phys. 114 (2009) 837–841.
[20] K.-W. Nam, C.-W. Lee, X.-Q. Yang, B.W. Cho, W.-S. Yoon, K.-B. Kim, J. Power Sources 188 (2009) 323–331.
[21] V. Subramanian, H. Zhu, B. Wei, Electrochem. Commun. 8 (2006) 827–832.
[22] G.-X. Wang, B.-L. Zhang, Z.-L. Yu, M.Z. Qu, Solid State Ionics 176 (2005) 1169–1174.
[23] Y. Wang, H. Liu, X. Sun, I. Zhitomirsky, Scripta Mater. 61 (2009) 1079–1082.
[24] X. Xie, L. Gao, Carbon 45 (2007) 2365–2373.
[25] J. Yan, Z. Fan, T. Wei, J. Cheng, B. Shao, K. Wang, L. Song, M. Zhang, J. Power Sources 194 (2009) 1202–1207.
[26] J. Liu, J. Essner, J. Li, Chem. Mater. 22 (2010) 5022–5030.
[27] W.D. Zhang, J. Chen, Pure Appl. Chem. 81 (2009) 2317–2325.
[28] H. Zhang, G.P. Cao, Z.Y. Wang, Y.S. Yang, Z.J. Shi, Z.N. Gu, Nanoletters 8 (2008) 2664–2668.
[29] N. Yao, V. Lordi, S.X.C. Ma, E. Dujardin, A. Krishnan, M.M.J. Treacy, T.W. Ebbesen, J. Mater. Res. 13 (1998) 2432–2437.
[30] C.E. Banks, X. Ji, A. Crossley, R.G. Compton, Electronalaysis 18 (2006) 2137–2140.
[31] J. Robertson, Mater. Sci. Eng. R37 (2002) 129–281.
[32] A. Jorio, M.A. Pimenta, A.G. Souza Filho, R. Saito, G. Dresselhaus, M.S. Dresselhaus, New J. Phys. 5 (2003), 139.1-139.17.
[33] C. Thomsen, Phys. Rev. B 61 (2000) 4542–4544.
[34] L. Valentini, J.M. Kenny, J. Appl. Phys. 92 (2002) 6188–6194.
[35] A. Malak-Polaczyk, C. Matei-Ghimbeu, C. Vix-Guterl, E. Frackowiak, J. Solid State Chem. 183 (2010) 969–974.
[36] A. Yuan, X. Wang, Y. Wang, J. Hu, Energ. Convers. Manage. 51 (2010) 2588–2594.